AIAA JOURNAL
Vol. 50, No. 12, December 2012

Carbuncle Phenomena and Other Shock Anomalies in Three Dimensions

Keiichi Kitamura* and Eiji Shima†
Japan Aerospace Exploration Agency, Kanagawa 252-5210, Japan
and
Philip L. Roe‡
University of Michigan, Ann Arbor, Michigan 48109

DOI: 10.2514/1.J051227

Hypersonic flow computations have proved to be very troublesome due to the appearance of shock anomalies (instabilities and oscillations) such as carbuncle phenomenon. These anomalies are categorized into one-dimensional and multidimensional modes, and these modes both arise from many factors and their combinations. Accurate prediction of hypersonic heating, a key issue in hypersonic flow computations, is therefore challenging especially for three dimensions. In the present study, we focus on three-dimensional shock anomalies and heating motivated by the following reasons. 1) Intuitively, multidimensional shock anomalies are considered to develop more likely in three dimensions than in two dimensions, but it cannot be proved mathematically nor has it been numerically demonstrated; specifically, it is not clear yet whether the third dimension plays another role that is absent in two dimensions. 2) Most proposed remedies for multidimensional anomalies had been tested in one- or two-dimensional setups in the literature, but it is not guaranteed whether such multidimensional dissipations actually work well in three dimensions. 3) It is already known to be troublesome to extend some multidimensional methods developed in two dimensions to three dimensions. The numerical results show that three-dimensional anomalies are too complicated to be predicted from their two-dimensional counterparts and that they can either be partly removed or, even worse, enhanced by multidimensional dissipations. Therefore, robustness of a numerical method that worked well in two dimensions may not be preserved in three dimensions.

Nomenclature

C_p	=	pressure coefficient
c_p	=	specific heat at constant pressure
E	=	total energy
$\mathbf{E}_k$, $\mathbf{F}_k$	=	inviscid and viscous flux vectors in k direction ($k = 1, 2, 3$, corresponding to x, y, z, respectively)
H	=	total enthalpy
M	=	Mach number
Pr	=	0.72, Prandtl number
p	=	pressure
q	=	heat-transfer rate
R	=	0.1 m, radius of sphere
Re	=	Reynolds number
T	=	temperature
u, v, w	=	velocity components in Cartesian coordinates
V	=	velocity
x, y, z	=	Cartesian coordinates
γ	=	1.4, specific heat ratio
$\Delta_{\min}$	=	minimum grid spacing (near the wall)
κ	=	$\mu c_p/Pr$, thermal conductivity
μ	=	molecular viscosity
ρ	=	density
ϕ	=	angle from the nose (where $\phi = 0$) of cylinder or sphere

Subscripts

cell	=	value based on the minimum grid spacing
F-R	=	Fay-Riddell's predicted value
w	=	value on the wall
∞	=	freestream value
0	=	stagnation value
1	=	post-shock value
2	=	pre-shock value

Received 16 February 2011; revision received 28 December 2011; accepted for publication 4 January 2012.

*Research Fellow of Japan Society for the Promotion of Science (JSPS), JAXA's Engineering Digital Innovation (JEDI) Center, 3-1-1 Yoshinodai, Chuo; currently Assistant Professor, Department of Aerospace Engineering, Nagoya University, 1 Furo-cho, Chikusa, Nagoya, Aichi 464-8603, Japan. Member AIAA.

†Senior Researcher and Director, JAXA's Engineering Digital Innovation (JEDI) Center, 3-1-1 Yoshinodai, Chuo. Member AIAA.

‡Professor, Department of Aerospace Engineering. Fellow AIAA.

I. Introduction

HYPERSONIC flow computations have proved to be very troublesome due to appearance of shock anomalies (instabilities or oscillations) such as carbuncle phenomenon [1]: Fig. 1 for the case in typical two-dimensional (2-D) domain, and Fig. 2 for 2-D normal shock. Although we are aware that classifications of such anomalous solutions are scattered among the researchers [2–6], we show in Table 1 what we currently believe to be the most convincing idea, in which the carbuncles are categorized into multidimensional (MD) instabilities. At any rate, all those anomalies are known to arise from the following factors and their combinations [7–9]: flow conditions (Mach number, Reynolds number, and the ratio of specific heats), mesh (size, aspect ratio, etc.), and numerical methods (flux function, accuracy, etc.). In particular, the authors [9] recently reported that any flux functions can lead to those anomalous solutions, depending on the shock location relative to grid lines. Moreover, they made clear that there are at least two causes of the shock anomalies: one of these is a one-dimensional (1-D) effect, and the other is MD. The former appeared to be alleviated by adding (1-D) dissipation to the shock-normal direction, whereas the latter could usually be suppressed by MD dissipation in the shock-perpendicular (transverse) direction [10–18]. However, when both of the two causes arise at the same time, these dissipations do not work well. Thus, a flux function that is free from those two kinds of anomalies is needed. We do of course

have several flux functions that can be tuned by an experienced user to solve many specific problems. In practice, "the devil you know" may be preferable to the one that you do not.

Accurate prediction of hypersonic heating, a key issue in hypersonic flow computations, is therefore challenging [19,20], especially for three-dimensional (3-D) complex geometries. For heating computations, the authors [21] suggested the use of flux functions satisfying the following three properties: 1) shock stability/robustness (i.e., free from both 1-D and MD anomalies), 2) conservation of total enthalpy (and hence total temperature), and 3) an ability of the Euler solver to sharply resolve contact discontinuities. This is necessary if the associated Navier–Stokes solver is to resolve boundary layers (and hence temperature gradients) economically.

It turned out that, unfortunately, we had no flux perfectly satisfying all the properties. Nevertheless, the criteria introduced therein for hypersonic heating computations and the classification of Euler fluxes are considered useful pieces of information in choosing/developing Euler fluxes (for details, please see [21]).

In our previous work [9,21], we focused on 1-D and 2-D issues; in the present study, we will extend these discussions to three dimensions, motivated by the following reasons.

1) Intuitively, MD shock anomalies are considered to develop more likely in 3-D, but this cannot be proved mathematically, nor has it been numerically demonstrated. Specifically, it is not still clear whether the third dimension (added dimension into a 2-D setup) introduces behavior that is absent in 2-D.

2) Most of the proposed remedies [10–14] for shock anomalies had been tested in 1-D and 2-D setups in the literature with the claim that "3-D extension is straightforward." It is true in a mathematical sense that the concept can be generalized, but taking into account the previous observation, it is hard to guarantee continued success.

3) It is already known to be troublesome to extend some of MD methods developed from 2-D considerations to 3-D. Yoon et al. [22], for instance, stated in their recent work that the difficulties in 3-D extension encountered by their 2-D-based limiter stem from the fact that "cells do not belong to the same plane." Balsara [23] argued that one form of the Harten–Lax–van Leer–Einfeldt (HLLE) Riemann solvers is too dissipative in MD, while a simple extension of the original 1-D flux to multidimensions limits Courant number and only works for Euler equations. Moreover, from the authors' experience, an MD hybrid flux using two vectors of normal and parallel to the shock [12] can face a difficulty in determining the two shock-parallel directions in 3-D space, even though one of those vectors can be (arbitrarily) defined; the problem was that the needed dissipation to suppress shock anomalies may differ from one direction to another.

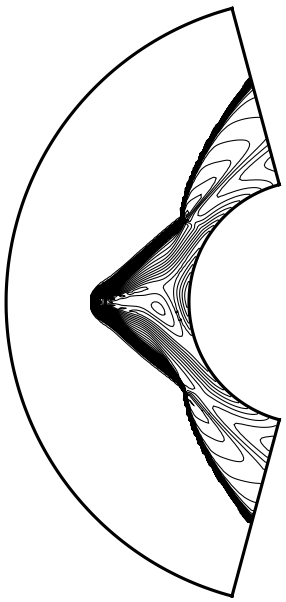

Fig. 1 2-D converged, carbuncle solution.

Table 1 Shock anomalies

Anomalies	Oscillations	Instabilities
1-D	Y (only in time)	N (not observed yet)
MD	Y (both in time and space)	Y (carbuncle)

We will extend and conduct our previous numerical experiments [9,21] along with benchmark tests in [20,24] in 3-D for popular Euler fluxes. As in our previous work, we took great care to eliminate any asymmetry from the grid or the initial data, and no artificial perturbations were introduced in an attempt to trigger instability. Therefore, we believe that all of the anomalies that we observe arise initially as computational instabilities driven by rounding error. This accounts for the fact that many phenomena took thousands of iteration to become visible. In practice, they might arise much earlier in response to nonsmoothness of the data. Finally, we will try to summarize 3-D shock anomalies stressing both the similarities and differences with their 2-D counterparts.

II. Computational Method

A. Governing Equations

The governing equations are the compressible Euler and Navier–Stokes equations.Euler:

$$\frac{\partial \mathbf{Q}}{\partial t} + \frac{\partial \mathbf{E}_k}{\partial x_k} = 0 \tag{1a}$$

Navier–Stokes:

$$\frac{\partial \mathbf{Q}}{\partial t} + \frac{\partial \mathbf{E}_k}{\partial x_k} = \frac{\partial \mathbf{F}_k}{\partial x_k} \tag{1b}$$

$$\mathbf{Q} = \begin{bmatrix} \rho \\ \rho u_i \\ \rho E \end{bmatrix}, \quad \mathbf{E}_k = \begin{bmatrix} \rho u_k \\ \rho u_i u_k + p\delta_{ik} \\ \rho u_k H \end{bmatrix}, \quad \mathbf{F}_k = \begin{bmatrix} 0 \\ \tau_{ik} \\ u_j \tau_{jk} + \kappa \frac{\partial T}{\partial x_k} \end{bmatrix} \tag{2}$$

$$\tau_{jk} = \mu\left(\frac{\partial u_j}{\partial x_k} + \frac{\partial u_k}{\partial x_j}\right) + \lambda \frac{\partial u_l}{\partial x_l}\delta_{jk} \tag{3}$$

where ρ is density, u_i are velocity components in Cartesian coordinates, E is total energy, p is pressure, H is total enthalpy ($H = E + (p/\rho)$), and T is temperature. The working gas is assumed to be air approximated by the calorically perfect gas model with the specific heat ratio $\gamma = 1.4$. The Prandtl number is $Pr = 0.72$. The viscosity μ is calculated by Sutherland's formula, and Stoke's hypothesis is employed, that is $\lambda = -2\mu/3$.

B. Computational Method

The following methods are used for computations herein, if not mentioned otherwise.

As for spatial discretization, the primitive variables at each cell interface are simply interpolated from the cell-center values (first

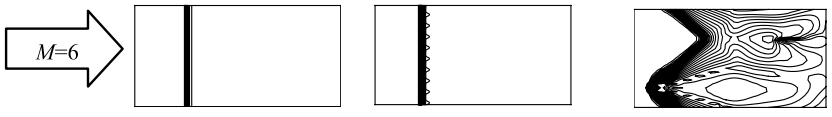

a) b) c)

Fig. 2 Typical solutions for $1\frac{1}{2}$-D test: a) successful (physically correct and stable), b) unacceptable (shock 'oscillation'), c) failure (shock 'instability,' called 'carbuncle').

Table 2 Classification of Euler fluxes based on three properties for hypersonic heating [21]

Flux functions	Group 1 Roe (E-Fix)	Group 2 Van Leer	Group 3 AUSM+, AUSMPW+
1) Shock Stability/ Robustness	Poor	Good	Fair
2) H preserving	N	N	Y
3) B-L Resolution	Y	N	Y

order) for inviscid cases, because shock anomalies tend to develop more likely in first order rather than in second order [9] (cases 1 and 2, explained later), or to second-order accuracy by Van Albada-limited [25] MUSCL reconstruction [26] for viscous cases (cases 3 and 4, again explained later). The Van Albada limiter, one of the most commonly used limiters, is selected because of its better convergence performance in general. Then, inviscid fluxes at the cell interface are calculated from Roe (E-Fix) (Roe [27] with Harten's entropy fix [28]), Van Leer's flux vector splitting (FVS) [29], AUSM+ [30], or AUSMPW+ [11]. Roe's flux-difference splitting (FDS), representing FDS schemes in group 1, has low dissipation, although it is known to be vulnerable to shock anomalies (e.g., carbuncle phenomenon) [7,9]. Van Leer's FVS (representing FVS schemes in group 2), on the other hand, is known to be almost free from such shock anomalies but actually exhibits them in extreme cases [21]. AUSM+ (group 3), which can be regarded as a mixture of FDS and FVS and so represents group 3, is more stable than Roe's flux [2,3], and preserves constant enthalpy in steady flows, although it also suffers from shock anomalies under certain conditions [9,21]. AUSMPW+ (group 3) is an improved AUSM+ equipped with a multidimensional dissipation term. These fluxes were categorized as in Table 2 [21]. Other MD fluxes [12–15] are also of interest, but in this paper we will focus on only representative fluxes chosen from each group. However, it should be admitted that our groups may not be ideally chosen. Hänel's flux [31], a variant of Van Leer's FVS having total enthalpy conserving property, is omitted because it reportedly [21] behaves in almost the same manner as Van Leer's FVS. The selected fluxes are briefly described in 2-D forms next.

Roe (E-Fix) [27,28]:

$$\mathbf{F}_{1/2} = \frac{1}{2}(\mathbf{F}_L + \mathbf{F}_R) - \frac{1}{2}\mathbf{R}|\hat{\mathbf{\Lambda}}|\mathbf{L}\,\mathbf{\Delta Q} \tag{4}$$

The $\hat{}$ stands for Roe-averaged values. $\mathbf{R}$ and $\mathbf{L}$ are right and left eigenvectors, respectively, and $\mathbf{\Lambda}$ is the diagonal matrix of characteristic speeds, with entropy-fix $\lambda_{1,4} \to 0.5(\lambda_{1,4}^2/\varepsilon + \varepsilon)$ if $|\lambda_{1,4}| < \varepsilon$, $\varepsilon = 0.2$.

Van Leer's FVS [29]:

$$\mathbf{F}^{\pm}_{1/2} = \begin{cases} \frac{1}{2}[1 \pm \text{sign}(M)]\mathbf{F}_R, & \text{if } M < -1 \\ \frac{1}{2}[1 \pm \text{sign}(M)]\mathbf{F}_L, & \text{if } M > 1 \\ \pm\frac{\rho}{4c}(u \pm c)^2\left[1, \frac{(\gamma-1)u \pm 2c}{\gamma}, v, \frac{[(\gamma-1)u \pm 2c]^2}{2(\gamma^2-1)} + \frac{v^2}{2}\right]^T, & \text{otherwise} \end{cases} \tag{5}$$

AUSM+ [30]:

$$\mathbf{F}_{1/2} = (M_L^+|_{\beta=1/8} + M_R^-|_{\beta=1/8})a_{1/2}\mathbf{\Phi}_{1/2} + (P_L^+|_{\alpha=3/16}\mathbf{P}_L + P_R^-|_{\alpha=3/16}\mathbf{P}_R),$$
$$\mathbf{\Phi} = (\rho, \rho u, \rho v, \rho H)^T, \qquad \mathbf{P} = (0, p, 0, 0)^T \tag{6a}$$

$$M^{\pm}|_{\beta} = \begin{cases} \frac{1}{2}(M \pm |M|), & \text{if } |M| \geq 1 \\ \pm\frac{1}{4}(M \pm 1)^2 \pm \beta(M^2-1)^2, & \text{otherwise} \end{cases} \tag{6b}$$

$$P^{\pm}|_{\alpha} = \begin{cases} \frac{1}{2}[1 \pm \text{sign}(M)], & \text{if } |M| \geq 1 \\ \frac{1}{4}(M \pm 1)^2(2 \mp M) \pm \alpha M(M^2-1)^2, & \text{otherwise} \end{cases} \tag{6c}$$

where $a_{1/2} = \min(\tilde{a}_L, \tilde{a}_R)$, $\tilde{a} = a^{*2}/\max(a^*, |u|)$

Table 3 Test cases and results, S (successful: stable and symmetric), U (unacceptable: oscillatory, asymmetric, or poor prediction of heating), and F (failure: carbuncle or diverged).

Cases	Euler fluxes	2-D				3-D		
		1A, $\varepsilon = 0.0$	1A, $\varepsilon = 0.5$	1B, $\varepsilon = 0.0$	1C, $\varepsilon = 0.0$	1C, $\varepsilon = 0.5$	1D, $\varepsilon = 0.0$
1) Normal shock $M = 6$	Roe (E-Fix	F (carbuncle)	F (carbuncle)	——	F (carbuncle)	F (carbuncle)	——
	Van Leer	S	S	F (carbuncle)	S	S	S
	AUSM+	S	U (not converged)	——	S	U (not converged)	——
	AUSMPW+	S	S	F (carbuncle)	S	S	F (carbuncle)
		$\delta = 0.0$	$\delta = 0.5$		$\delta = 0.0$	$\delta = 0.5$	
2) Cylinder $M = 6$	Roe (E-Fix)	F (carbuncle)	F (carbuncle)		F (carbuncle)	F (carbuncle)	
	Van Leer	S	S		S	——	
	AUSM+	S	S		S	——	
	AUSMPW+	S	S		S	——	
		$\delta = 0.0$	$\delta = 0.5$		$\delta = 0.0$	$\delta = 0.5$	
3) Viscous cylinder, $M = 17$	Roe (E-Fix)	S	U (oscillatory)		U (oscillatory)	F (diverged)	
	Van Leer	U (severely low heating)	U (Severely low heating)		U (severely low heating)	U (severely low heating)	
	AUSM+	U (not converged)	U (not converged)		U (not converged)	U (not converged)	
	AUSMPW+	S	S		S	S	
4) Viscous sphere, $M = 12$	Roe (E-Fix)					F (diverged)	
	Van Leer					U (severely low heating)	
	AUSM+					U (asymmetrical)	
	AUSMPW+					U (asymmetrical)	

AUSMPW+ [11]:

$$\mathbf{F}_{1/2} = \bar{M}_L^+ c_{1/2}\mathbf{\Phi}_L + \bar{M}_R^- c_{1/2}\mathbf{\Phi}_R + (P_L^+|_{\alpha=0}\mathbf{P}_L + P_R^-|_{\alpha=0}\mathbf{P}_R),$$
$$\mathbf{\Phi} = (\rho, \rho u, \rho v, \rho H)^T, \qquad \mathbf{P} = (0, p, 0, 0)^T \tag{7a}$$

$$\text{If } \; m_{1/2} = M_L^+ + M_R^- \geq 0 \tag{7b}$$

$$\bar{M}_L^+ = M_L^+ + M_R^- \cdot [(1-w)\cdot(1+f_R) - f_L],$$
$$M_R^- = M_R^- \cdot w \cdot (1+f_R) \tag{7c}$$

otherwise,

$$\bar{M}_L^+ = M_L^+ \cdot w \cdot (1+f_L),$$
$$M_R^- = M_R^- + M_L^+ \cdot [(1-w)\cdot(1+f_L) - f_R] \tag{7d}$$

where

$$w = 1 - \min\left(\frac{p_L}{p_R}, \frac{p_R}{p_L}\right)^3 \tag{7e}$$

$$f_{L,R} = \begin{cases} \left(\frac{p_{L,R}}{p_S} - 1\right) \min\left(1, \frac{\min(p_{1,L}, p_{1,R}, p_{2,L}, p_{2,R})}{\min(p_L, p_R)}\right)^2, & p_S \neq 0 \\ 0, & \text{otherwise} \end{cases} \tag{7f}$$

and $p_S = P_L^+ p_L + P_R^- p_R$.

Viscous fluxes are computed by using second-order central difference, whereas, for time integration, first-order Euler explicit method (for inviscid cases) or LU-SGS (for viscous cases) is employed. No turbulence model or real gas model has been used. Detailed information of the solver with regard to formulations and discretizations is found in [32].

III. Two- and Three-Dimensional Tests for Hypersonic Shock Anomalies

In this section, we perform and compare 2-D and 3-D numerical tests, including a few reviewed results [9,12] that are essential to the present discussions. As noted in the Introduction, care was taken in all cases to ensure that the grids and initial data were symmetrical within rounding error. Euler equations are solved by a finite-volume code first order both in time and space. All the test cases and results are summarized in Table 3.

A. Test 1: Planar Shock

1. 2-D

These cases were already conducted extensively in [9,21], but here we extract only limited results that are essential to the present discussions.

Test 1A: The grid consists of 50×25 square cells, as shown in Fig. 3a. The numerical conditions, e.g., $M_\infty = 6.0$, 40,000 steps with CFL = 0.5, are the same in [9]. The initial shock position parameter ε (see [9] or the description in Sec. III.B), alternating between ε and δ, is taken as 0.0 or 0.5; the initial shock is imposed exactly on a cell interface when $\varepsilon = 0.0$, and at the cell-center when $\varepsilon = 0.5$; see Fig. 3a. Typical results are shown in Fig. 2. The example result by using Van Leer's FVS is shown in Fig. 3b and exhibits no evidence of shock anomalies. The results from other fluxes are summarized in Table 3.

As shown in [9], the mechanisms of MD shock anomalies are distinct from their 1-D counterpart, although the former anomalies are related to the latter; 1-D shock oscillation appears depending on the relative positioning of the shock to the grid line, while the MD oscillations can be triggered by 1-D oscillations in certain conditions. Detailed explanations for 1-D and 2-D anomalies are found in [9,21].

Test 1B: The grid was extended to 50×250 cells, as shown in Fig. 4a. The computations were conducted 200,000 steps with the other conditions remained [21]. The MD shock irregularities can develop if the numbers of grid points is increased in the shock perpendicular direction [21], as shown in Fig. 4b. This suggested the possibility that the increment of the grid points is related to increment of degrees of freedom for numerical errors to develop.

2. 3-D

Test 1C: The grid consists of 10 of the 2-D grids (test 1A, Fig. 3a) stacked in the additional dimension ($50 \times 25 \times 10$ cells, Fig. 5a).

Test 1D: The grid consists of 10 of the 2-D grids (test 1B, Fig. 4a) stacked in the additional dimension ($50 \times 250 \times 10$ cells).

All the cells are isotropic (meaning that the same distances are maintained between grid points along each mesh line), and the computational conditions are the same as the 2-D case. Only selected results will be presented next.

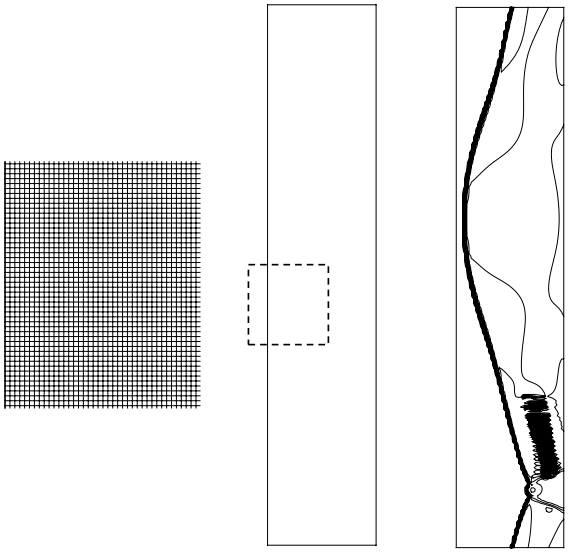

a) **b)**

Fig. 4 Modified $1\frac{1}{2}$-D test (test 1B, 50 × 250 cells), a) grid, b) result of Van Leer's FVS [21].

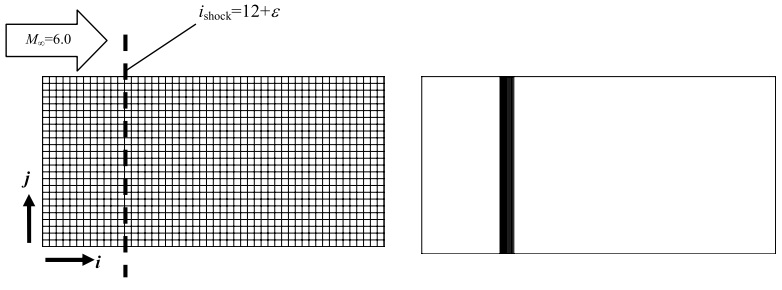

a) **b)**

Fig. 3 $1\frac{1}{2}$-D steady shock test (test 1A, 50 × 25 cells), a) grid, b) result of Van Leer's FVS [9,21].

The results for test 1C are shown in Figs. 5–8. The Roe (E-Fix) (Fig. 5b) showed total breakdown (carbuncle) in three dimensions. The shock shape is irregular (i.e., the instability occurs in every direction). Results of Van Leer (Fig. 6), on the other hand, are stable as in the 2-D case (Fig. 3b). AUSM+ (Fig. 7) showed a stable result for $\varepsilon = 0.0$ but oscillatory for $\varepsilon = 0.5$, consistent with the 2-D cases in [21]. AUSMPW+ ($\varepsilon = 0.0$) initially showed regular oscillations in both directions (every bump has the same distance to each other, in contrast to Fig. 5b) perpendicular to the captured shock (Fig. 8a), but later the original planar shape was recovered (Figs. 8b and 8c). This recovery seems to be due to MD dissipation term in AUSMPW+. The similar behavior was already observed in 2-D and in another MD flux [12], but its effectiveness in 3-D has been confirmed at least in the current particular case.

Test 1D results are presented in Fig. 9 (Van Leer) and Fig. 10 (AUSMPW+). Astonishingly, the 3-D Van Leer results in Fig. 9 are more stable than the 2-D ones in Fig. 4b, but in conjunction with the previous hypothesis and the results in Figs. 3b and 4b, numerical dissipation added by cells in the third direction seemed to have a favorable effect in this case. The AUSMPW+ case (Fig. 10), in contrast, reached an unstable solution: small random wiggles appeared (that is, no regular pattern is observed) at 5000 steps (Figs. 10a and 10b); the breakdown of the shock shape occurred (during 5,000–10,000 steps, Fig. 10c); and finally, instability developed and remained at 40,000 steps (Fig. 10d). Note from Table 3 that the final state is similar to the corresponding 2-D results, rather than another 3-D result in test 1C (Fig. 8c). Therefore, the MD dissipation term in AUSMPW+ does not seem to be effective in cure of this '2-D dominant' anomaly.

B. Test 2: Hypersonic Flow over Blunt Body (Circular Cylinder)

1. 2-D

As in test 1 in 2-D, these cases are reviewed only for reference. The (shock-aligned) grid used in this test had originally been provided by Dr. Jeffery White et al. of NASA Langley Research Center [33]. This grid was constructed by identifying one grid line with the shock produced by an accurate shock-fitted solution, and is, rather surprisingly, a very difficult grid on which to capture a shock. After removing some small asymmetries from the grid that we received, we dilated the grid slightly so that the shock position now lay in general between two grid lines. In previous work we made use of various dilations, but here we used only two. When the parameter $\delta = 0$, we have the original grid as supplied, and when $\delta = 0.5$ the shock should

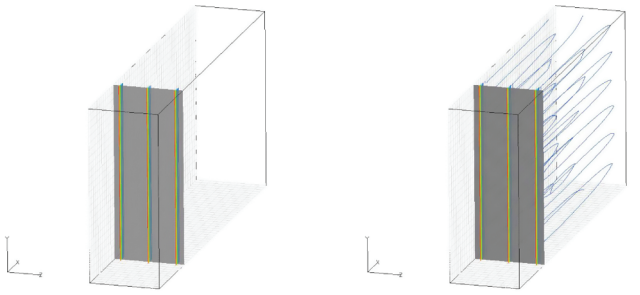

a) b)

Fig. 7 3-D steady planar shock test (test 1C, 50 × 25 × 10 cells), AUSM +, a) $\varepsilon = 0.0$, 40,000 steps, b) $\varepsilon = 0.5$, 40,000 steps.

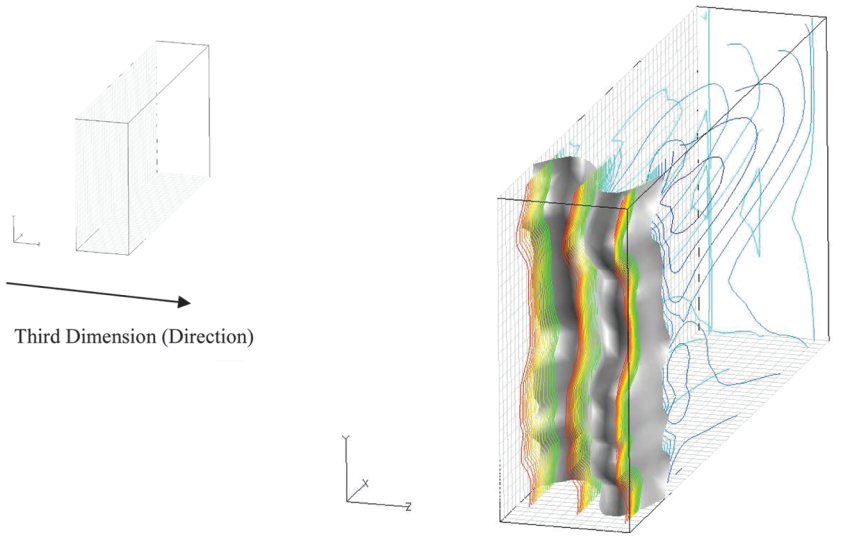

a) b)

Fig. 5 3-D steady planar shock test (test 1C, 50 × 25 × 10 cells), a) grid, b) Roe (E-Fix), $\varepsilon = 0.5$, 5000 steps; colors: Mach number; gray: $M = 1.5$ isosurface.

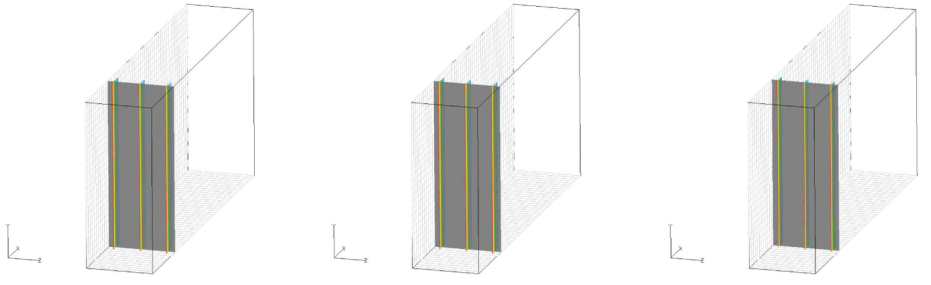

a) b) c)

Fig. 6 3-D steady planar shock test (test 1C, 50 × 25 × 10 cells), Van Leer, a) $\varepsilon = 0.0$, 5000 steps, b) $\varepsilon = 0.0$, 40,000 steps, c) $\varepsilon = 0.5$, 40,000 steps.

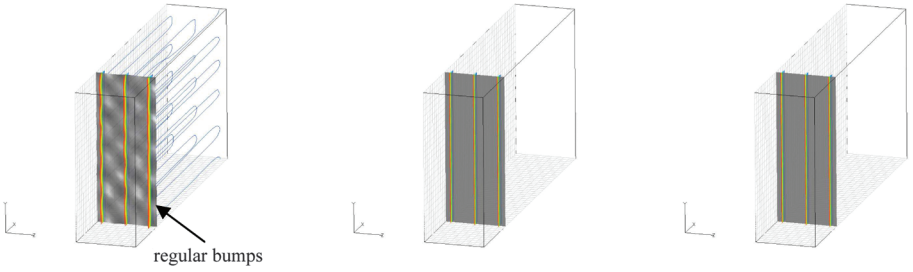

Fig. 8 3-D steady planar shock test (test 1C, 50 × 25 × 10 cells), AUSMPW+, a) $\varepsilon = 0.0$, 5000 steps, b) $\varepsilon = 0.0$, 10,000 steps, c) $\varepsilon = 0.0$, 40,000 steps.

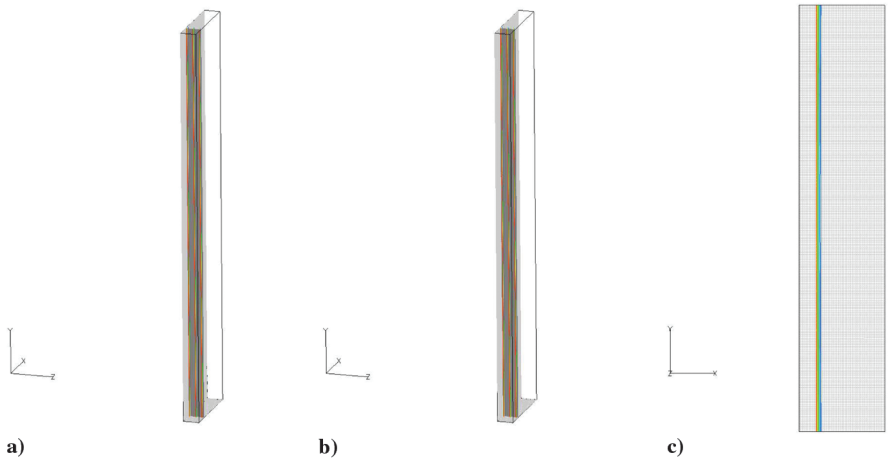

Fig. 9 3-D steady planar shock test (test 1D, 50 × 250 × 10 cells), Van Leer, a) $\varepsilon = 0.0$, 5000 steps, b) $\varepsilon = 0.0$, 40,000 steps, c) $\varepsilon = 0.0$, 40,000 steps (side view).

sit between two grid lines. The grid size and the computational conditions are: 1) Grid: 120 (circumferential) × 48 (wall-normal), 2) Courant-Friedrichs-Lewy (CFL) = 0.5, 3) Computational time steps: 50,000 steps, and 4) Flow condition: $M_\infty = 6.0$.

The grid and example result are shown in Figs. 11a. In the results, 1-D or (1-D-triggered) MD shock anomaly (these terminologies have been categorized in Table 1; see [21] for more detailed explanations) appeared on some grids, whereas it did not emerge on the other grids (Table 3). From this difference, it had been revealed that the relative positioning of the grid line to the shock, δ, played an important role, although this aspect of shock anomalies is not discussed in this section but later in the next section.

2. *3-D*

The grid in 2-D has been extended to three dimensions (100 cells in the third direction): 120 × 48 × 100 (evenly spaced)

The symmetry (reflection) condition is imposed at the spanwise boundaries, and the other computational conditions are the same as 2-D cases.

The results are shown in Figs. 11–13. Figure 11 is focused on the development of the '3-D carbuncle' for Roe (E-Fix) case. It is seen from the results that MD shock anomalies developed in every direction: More precisely, the 'carbuncle instability' seemed to have occurred in the 2-D slice (500 steps, Fig. 11b). By 1500 time steps, the carbuncle has reduced, but a spanwise oscillation has developed (Fig. 11c). Then, both of these anomalies combined (i.e., 2-D carbuncle and 3-D oscillations) until 5000 steps (Figs. 11d–11f), and this catastrophic solution remained unchanged to 50,000 steps (Fig. 11g), leaving 'bumps' randomly placed on the shock surface but showing the density residual decreased by more than seven orders of magnitude (Fig. 12a). Solutions of this kind, i.e., 'converged carbuncles,' are also reported in 2-D (Figs. 1 and 11a or [9,12]).

In contrast to the planar shock case (Fig. 5), the shock anomalies in this case seem to have developed in different modes in different directions, and also, in different rates. These differences seem to be due to the fact that the cells are totally the same from one slice to another, while within a slice the adjacent cells are different. Thus, there appeared to be two possibilities:

1) The 2-D carbuncle triggered 3-D oscillations (i.e., the appearance of the 3-D oscillations was totally dependent on the 2-D carbuncle).

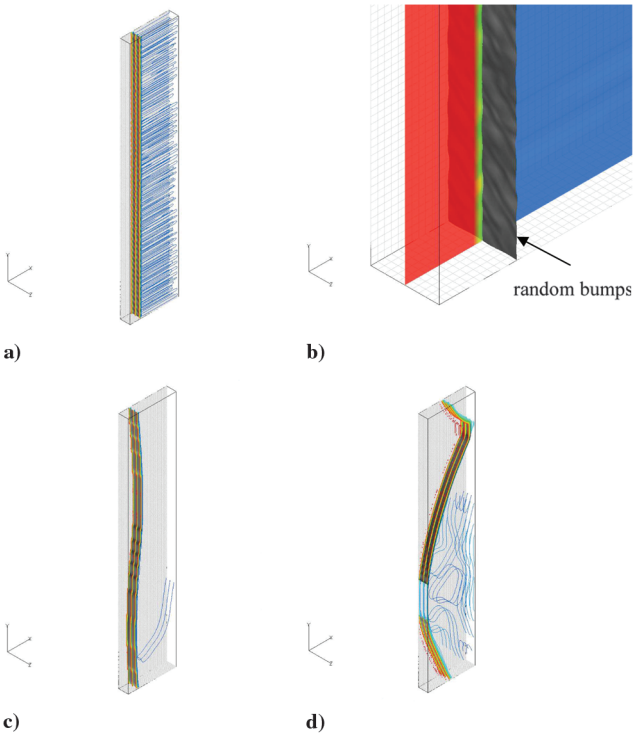

Fig. 10 3-D steady planar shock test (test 1D, 50 × 250 × 10 cells), AUSMPW+, a) $\varepsilon = 0.0$, 5000 steps, b) $\varepsilon = 0.0$, 5000 steps (blowup view), c) $\varepsilon = 0.0$, 10,000 steps, and d) $\varepsilon = 0.0$, 40,000 steps.

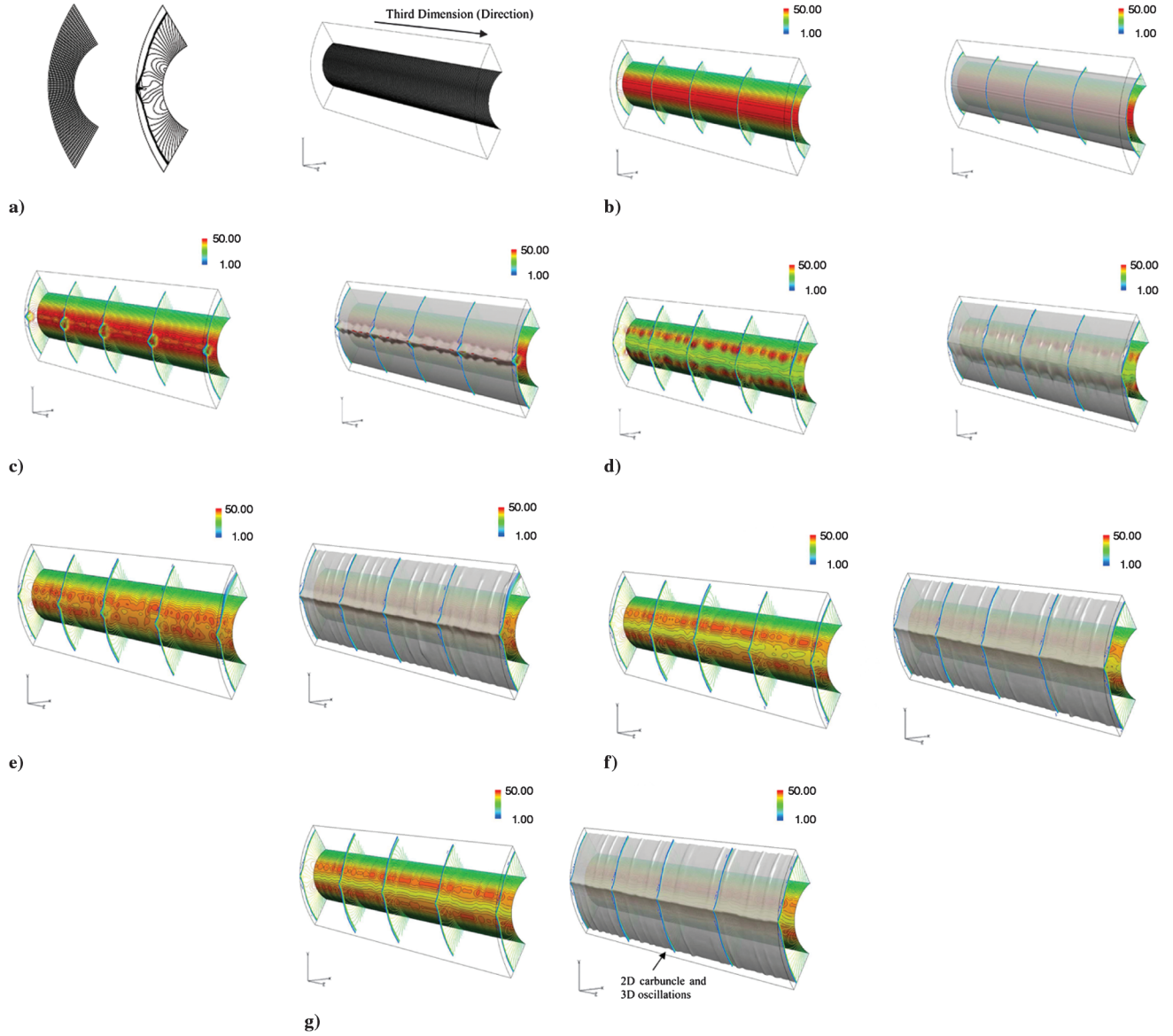

Fig. 11 a) Grids and reference 2-D 'carbuncle' result [9], and b–g) snapshots of developing 3-D carbuncle for circular cylinder, the Roe E-Fix; C_p contours (left; $0 < C_p < 50$) and iso-Mach-number surface (right; $M = 1.5$).

2) The 2-D carbuncle developed faster than 3-D oscillations (i.e., the 3-D oscillation gently and subliminally developed while the 2-D instability emerged).

We examined this by introducing and comparing $L2$ norms of 'velocity asymmetry,' defined as

$$|\Delta v| = |v_{\text{upper}} - (-v_{\text{lower}})| = |v(i,j,k) + v(i_{\max} + 1 - i, j, k)| \quad (8)$$

which is the measure of velocity difference between cells sharing the same x and z coordinates but having opposite signs in y, with a similar definition for $|w|$ (in the third dimension). According to Fig. 12, the instabilities both in y and z directions arose from the very

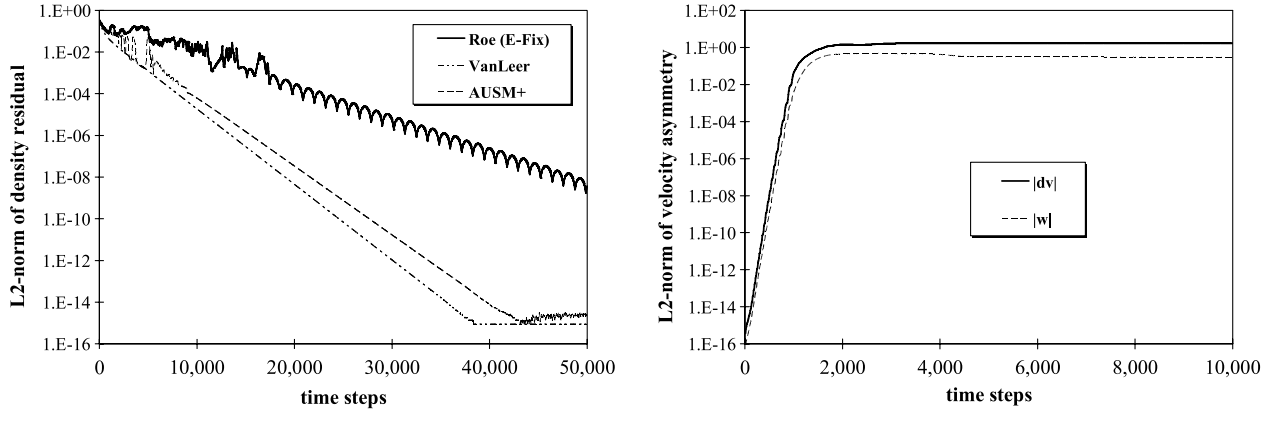

Fig. 12 Residual and asymmetry histories for 3-D circular cylinder ($M_\infty = 6.0$): a) density residual, and b) velocity asymmetry in v and w components.

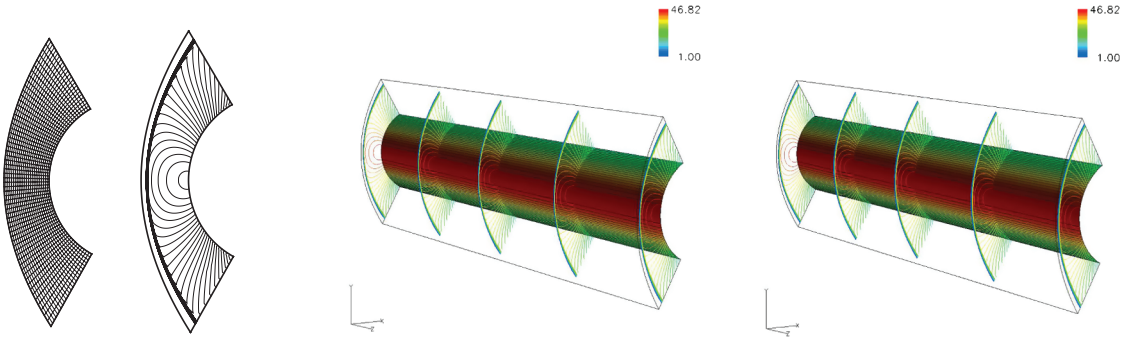

a) b) c)

Fig. 13 a) Grid and reference 2-D 'stable' result (AUSM+) [9], and 3-D results by C_p contours ($0 < C_p < 47$) for circular cylinder at 50,000 steps: b) AUSM+ and c) Van Leer's FVS.

beginning of the computation at the level of round-off errors, and they grew exponentially with time. Thus, it is difficult to conclude which of the previous hypotheses was right, but at least there is the possibility that 2-D and 3-D shock instabilities share the same cause, and that they developed in the same rate, yet in different appearances.

In AUSM+ or Van Leer results, however, as in 2-D case (Figs. 13a for AUSM+), no evidence of shock anomalies is seen (Figs. 13b and 13c): These flow patterns remained stable and symmetric even in the 3-D setup. They continued to do so, even when the third dimension was extended to give a grid size of $120 \times 48 \times 500$, though the results are omitted.

IV. Two- and Three-Dimensional Hypersonic Heating Tests for Navier–Stokes Codes

In this section, we carry out 2-D and 3-D viscous cases. Again, no initial perturbation is introduced. Navier–Stokes equations are

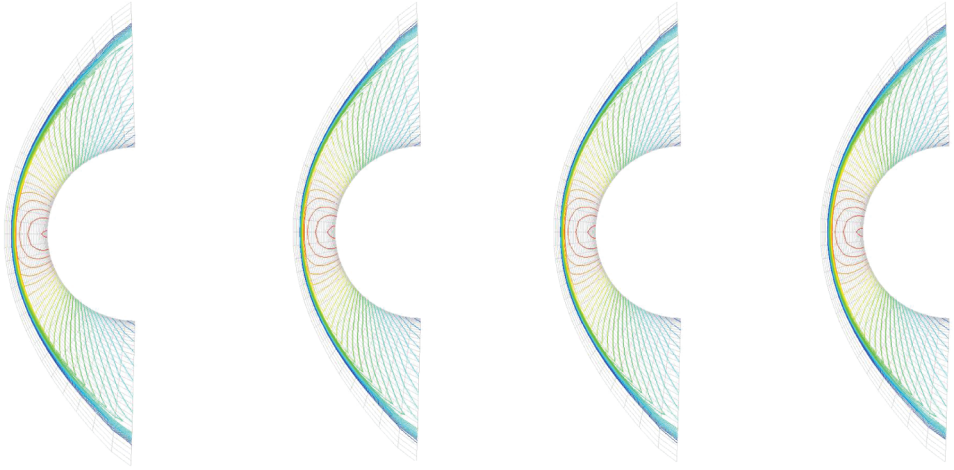

a) b) c) d)

Fig. 14 Pressure contours ($0 < P/P_\infty < 386$) for 2-D circular cylinder (second-order in space; freestream Mach number $M_\infty = 17$); original grid, $\delta = 0.0$; 30 × 64 cells: a) Roe (E-Fix), b) Van Leer, c) AUSM+, and d) AUSMPW+.

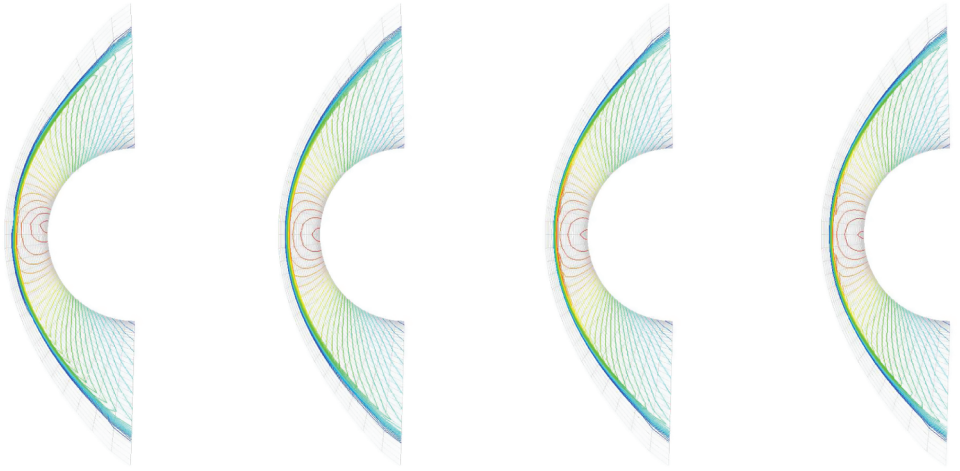

a) b) c) d)

Fig. 15 Pressure contours ($0 < P/P_\infty < 386$) for 2-D circular cylinder (second-order in space; freestream Mach number $M_\infty = 17$); modified (half-cell dilated) grid, $\delta = 0.5$; 30 × 64 cells: a) Roe (E-Fix), b) Van Leer, c) AUSM+, and d) AUSMPW+.

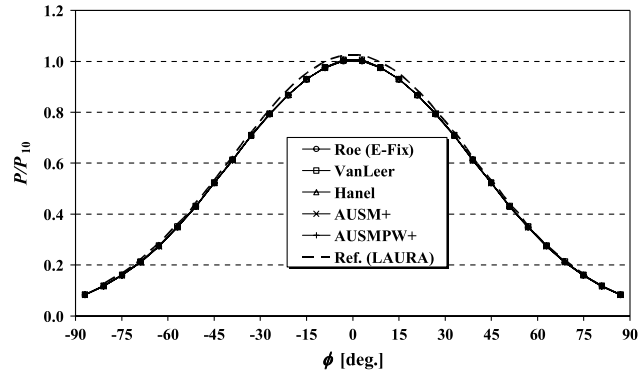

a)

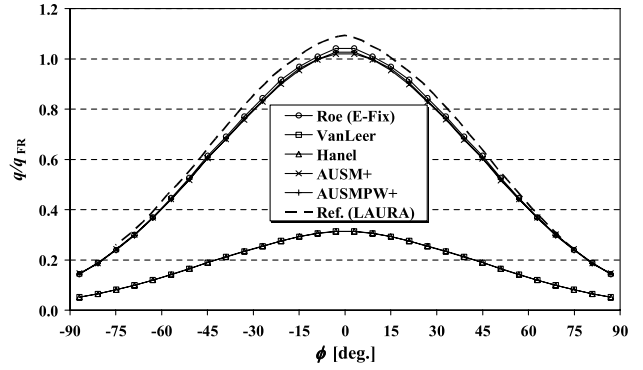

b)

Fig. 16 Surface pressure and heating profiles for 2-D cylinder (second-order in space; freestream Mach number $M_\infty = 12$); ooriginal grid, $\delta = 0.0$: a) pressure, and b) heating.

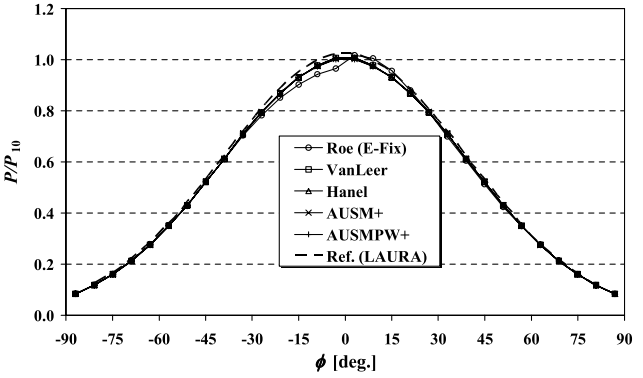

a)

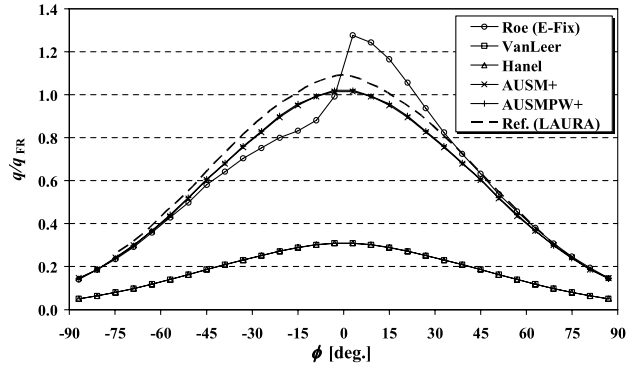

b)

Fig. 17 Surface pressure and heating profiles for 2-D cylinder (second-order in space; freestream Mach number $M_\infty = 12$); modified (half-cell dilated) grid, $\delta = 0.5$: a) pressure, and b) heating.

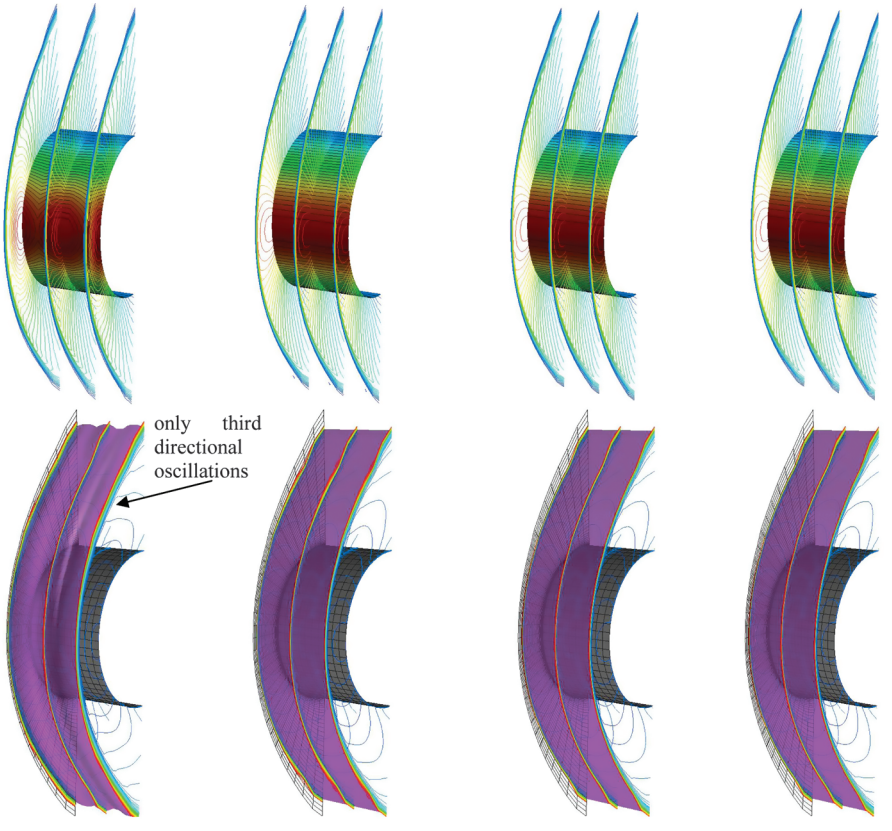

Fig. 18 Pressure (top; $0 < P/P_\infty < 390$) and Mach number (bottom; $0 < M_\infty < 17$) contours for 3-D circular cylinder (second-order in space; freestream Mach number $M_\infty = 17$): a) Roe (E-Fix), b) Van Leer, c) AUSM+, and d) AUSMPW+.

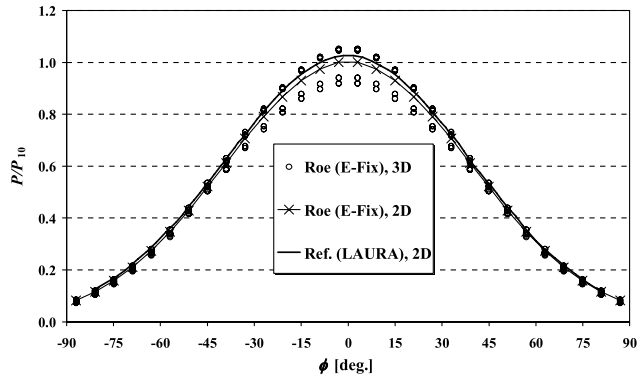

a)

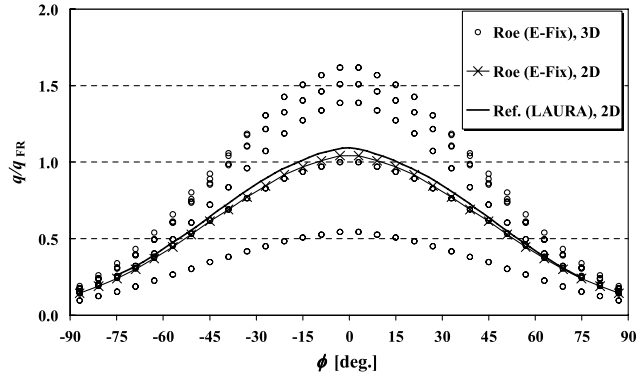

b)

Fig. 19 Surface pressure and heating profiles for 3-D cylinder (second-order in space; freestream Mach number $M_\infty = 12$); ooriginal grid, $\delta = 0.0$, Roe (E-Fix): a) pressure, and b) heating.

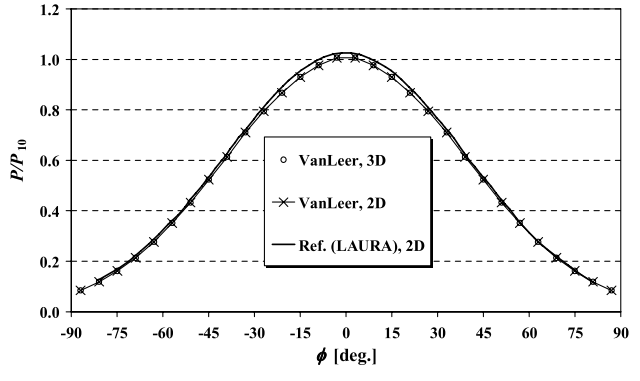

a)

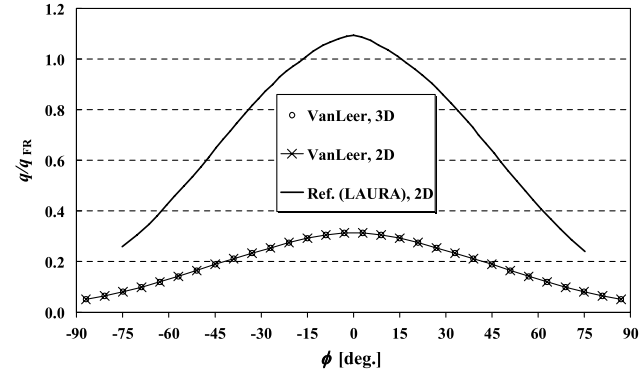

b)

Fig. 20 Surface pressure and heating profiles for 3-D cylinder (second-order in space; freestream Mach number $M_\infty = 12$); original grid, $\delta = 0.0$, Van Leer: a) pressure, and b) heating.

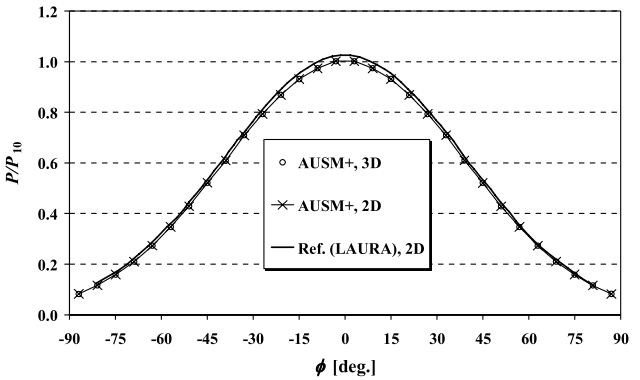

a)

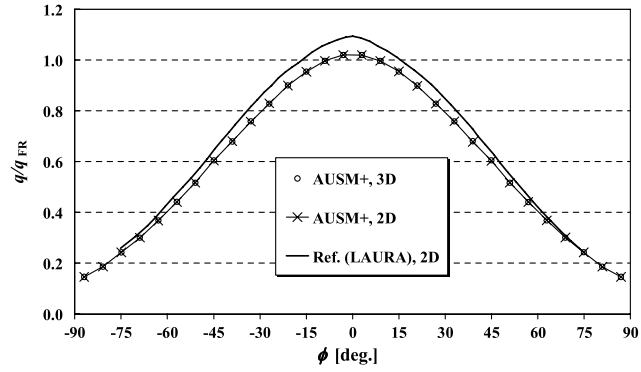

b)

Fig. 21 Surface pressure and heating profiles for 3-D cylinder (second-order in space; freestream Mach number $M_\infty = 12$); original grid, $\delta = 0.0$, AUSM+: a) pressure, and b) heating.

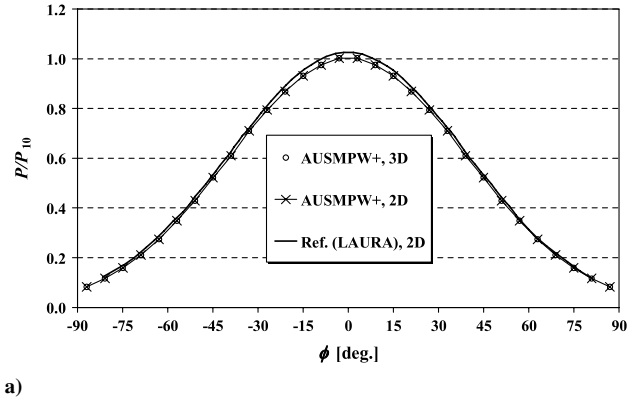

a)

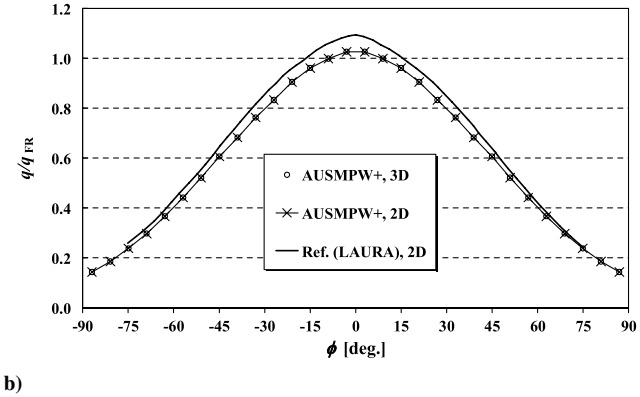

b)

Fig. 22 Surface pressure and heating profiles for 3-D cylinder (second-order in space; freestream Mach number $M_\infty = 12$); original grid, $\delta = 0.0$, AUSMPW+: a) pressure, and b) heating.

solved by a spatially second order finite-volume code with LU-SGS implicit time integration, and the results are included in Table 3.

A. Test 3: LAURA Benchmark Hypersonic Heating Test

1. 2-D

This is a viscous, hypersonic ($M_\infty = 17$) benchmark test used for LAURA (from Langley Aerothermodynamic Upwind Relaxation Algorithm, developed at NASA Langley for hypersonic flow simulations) and FUN3D codes [15], employing a shock-aligned grid. The grid was provided by Dr. Peter Gnoffo [34] as a 3-D mesh, but one slice of it was taken and used for the 2-D cases. Then, as in the test 2, we made the same modification on this grid, i.e., the 'original grid ($\delta = 0.0$)' was dilated a half-cell width as the 'modified grid ($\delta = 0.5$).' The computational conditions are given as follows: 1) Grid: 30×64, $\Delta_{\min} = 2.66\text{e}-6$ m; 2) CFL = 200; 3) Computational time steps: 100,000 steps; and 4) Flow conditions: $V_\infty = 5000$ m/s ($M_\infty = 17$), $Re = 376,930$ /m, $\rho_\infty = 0.001$ kg/m^3, $T_\infty = 200$ K, and $T_w = 500$ K.

With the previous setup, the cell Reynolds number is $Re_{\text{cell}} = 1.00$, the ratio of Pitot pressure to freestream pressure is $P_{10}/P_2 = 387.6$, and Fay-Riddell's [35] stagnation heating is 46.5 W/cm^2 (slightly smaller than LAURA-predicted value [15] of 52 W/cm^2).

Computed results are summarized in Figs. 14–17. One can see that Roe (E-Fix) suffered from shock anomaly in the modified grid (Fig. 15a), although the density residual dropped to $\mathcal{O}(-16)$ but not in the original grid. This anomaly clearly affected surface pressure and, more severely, surface heating rates (more than 20% overestimation); see Figs. 16a, 16b, 17a, and 17b. Other flux functions yielded symmetric and stable (at least eight orders drop in $L2$ norm of density residuals) solutions with the exception of AUSM+ (oscillatory results on either of the two grids, with only two orders reduction in residual). Van Leer resulted in severely poor predictions of heating, as expected. In addition, we point out here that a non-shock-aligned grid produced similar results as shown in [21].

2. 3-D

This is the 3-D case of the viscous, $M_\infty = 17$, hypersonic heating test, which was previously used, for example, in [15]. The grid was provided by Dr. Peter Gnoffo, as stated before. The grid system has $30 \times 64 \times 10$ cells with the symmetry condition at the spanwise boundaries, and the rest of the flow and computational conditions are the same as in the 2-D test.

The results for $\delta = 0.0$ are shown in Figs. 18–22. According to these figures, the Roe (E-Fix) case was affected by three-dimensional effect: the shock shape (Fig. 18a), surface pressure (about 5%, Fig. 18b), and heating (more than 50%, Fig. 18c) exhibited asymmetry in the crossflow direction (the third dimension), as in test 2. It is noteworthy that, in this case, the Roe (E-Fix) flux suffered from shock anomaly only in the third dimension and maintained the 2-D stable, symmetric solution (Fig. 14a) in each 2-D plane; this is in contrast to the example seen in Fig. 11 (test 2) in which anomalies appeared in every direction. This seems to show that sometimes an anomalous mode is suppressed by adding an extra dimension.

Other fluxes showed almost the same trends as in 2-D cases: Van Leer reached a converged to machine zero, $\mathcal{O}(-16)$, symmetric solution with surface heating underestimated; AUSM+ again suffered from numerical oscillations (only two orders residual drop); and AUSMPW+ solutions are indistinguishable from the 2-D solution.

The results for $\delta = 0.5$ are similar, only with one exception in Roe (E-Fix) case, which eventually blew up due to more severe oscillations, and hence are shown only in Table 3.

B. Test 4: 'Challenge' Problem for Sphere

1. 3-D

Although this problem is axisymmetric, it is solved on a fully 3-D grid and is therefore a genuinely 3-D test, referred to as a 'challenge' problem in [36] of viscous, hypersonic ($M_\infty = 12$) heating. A shock-aligned grid provided by Dr. Peter Gnoffo (through Dr. Bil Kleb) [37] was used. We conducted this test to demonstrate how difficult it is to obtain satisfactory heating profiles by existing methods in 3-D and how much MD terms work to improve the solutions. 1) Grid: $(45 \times 160 \times 125 =) 900,000$ cells + $(40 \times 40 \times 125 =) 200,000$ cells = 1,100,000 cells (Fig. 23a), 2) Radius: $R = 0.1$ m, 3) CFL = 200, 4) Computational time steps: 10,000 steps, and 5) Flow conditions: $V_\infty = 4167$ m/s ($M_\infty = 12$), $Re = 0.5e+6$ (based on radius R), $Re_{\text{cell}} = 5$ (based on minimum grid spacing $\Delta_{\min} = 1.\text{e}-6$ m), $\rho_\infty = 0.0216$ kg/m^3, $T_\infty = 300$ K, and $T_w = 800$ K.

With the previous setup, the ratio of Pitot pressure to freestream pressure is $P_{10}/P_2 = 185.9$, and Fay-Riddell's [35] stagnation heating is $q_{\text{F-R}} = 550.1$ W/cm^2 (smaller than 627 W/cm^2 in [36] and LAURA's prediction [15] of 590 W/cm^2). An example of computed flowfield is shown in Fig. 23b.

Roe (E-Fix) calculation diverged; thus, only the results of Van Leer, AUSM+, and AUSMPW+ are shown in Figs. 24 and 25, including the reference result from [15], where Gnoffo's version of Roe flux was used, which can control dissipation through multidimensional entropy fix. Surface pressure profiles shown in Fig. 24 are almost symmetric and in good agreement with reference data. AUSM+ yielded a very slight glitch at $\phi \approx 15$ deg (data at an angle ϕ stand for all the circumferential data in this test), but this is suppressed by MD term in AUSMPW+. Calculated heating rates, however, are totally underestimated (Van Leer) or strongly asymmetric (AUSM+ and AUSMPW+), as shown in

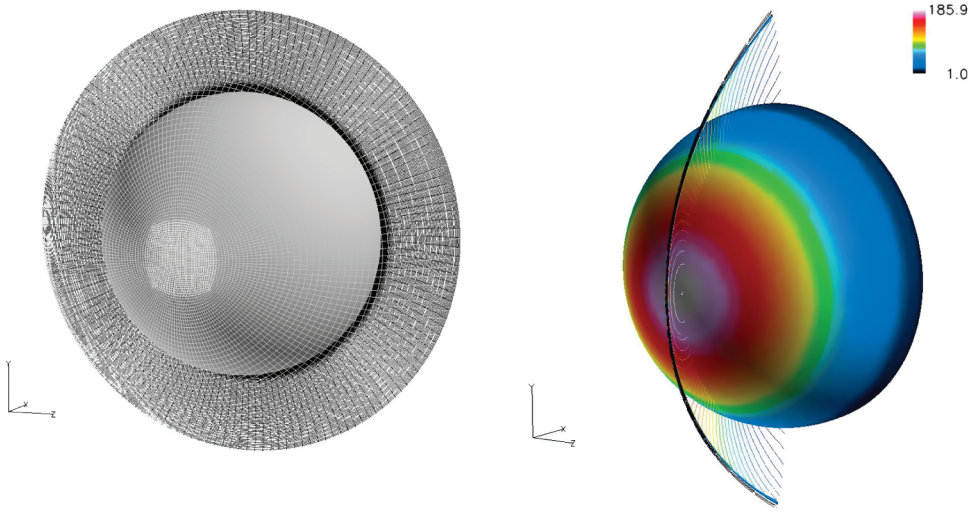

a) Grid **b) Pressure contours (AUSM+)**

Fig. 23 Computational grid and typical solution for $M_\infty = 12$ Candler's 'challenge' problem [38].

Fig. 25, even with this hexahedral mesh. Gnoffo [15] recently developed a multidimensional version of Roe flux, and the results shown therein were much better than the original Roe, though asymmetry was also seen in heating. AUSMPW+, despite having an MD dissipation term, was not much better than AUSM+ at preserving symmetry. In addition, the heating contours of our results (Figs. 25b and 25c) showed different shapes from [15] (or Fig. 25d), possibly due to the use of different implicit time-

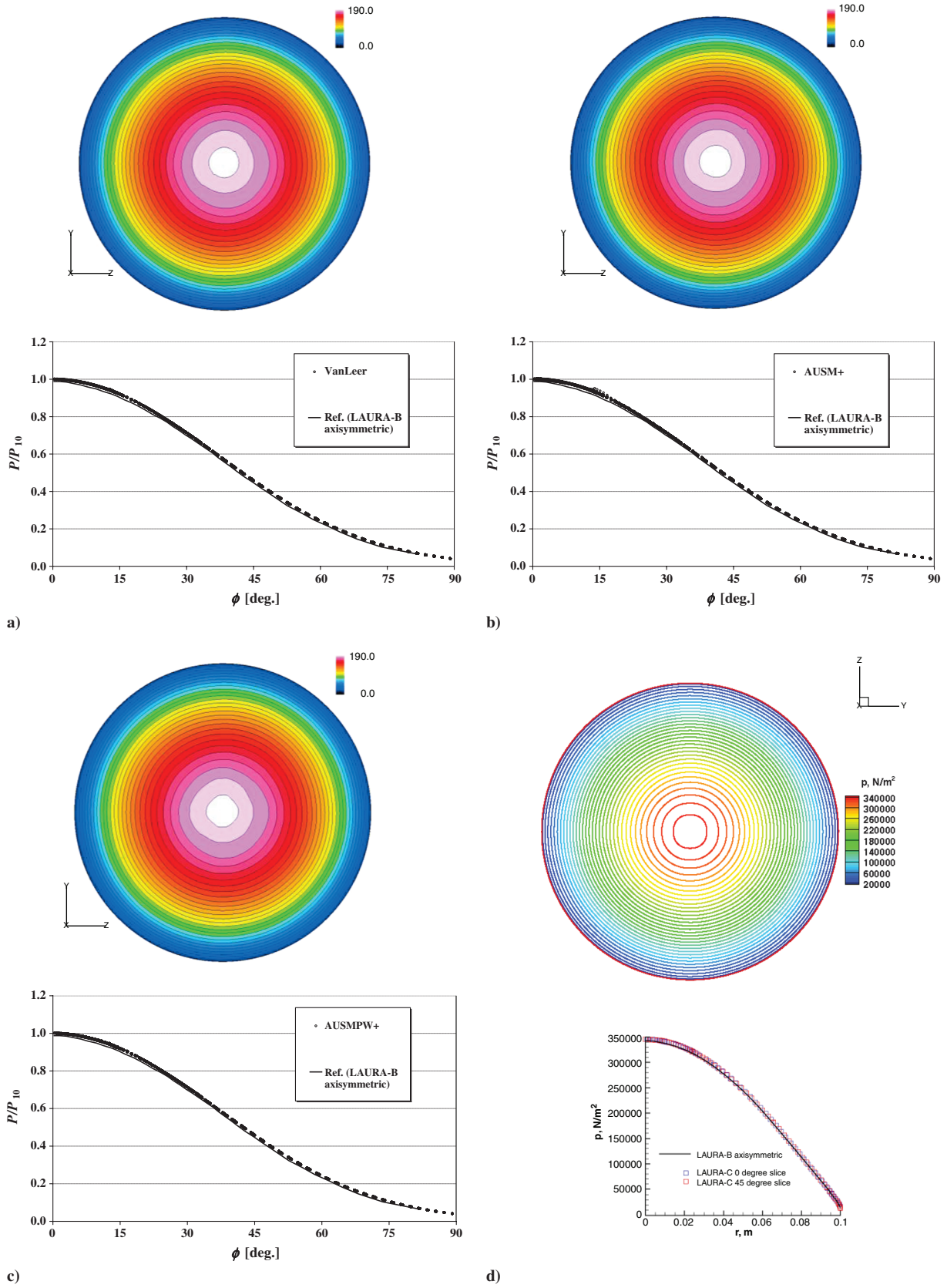

Fig. 24 Surface pressure contours (top; $0 < P/P_\infty < 190$) and profiles (bottom; 3-D, sphere): a) Van Leer, b) AUSM+, c) AUSMPW+, and d) [15], courtesy of Gnoffo.

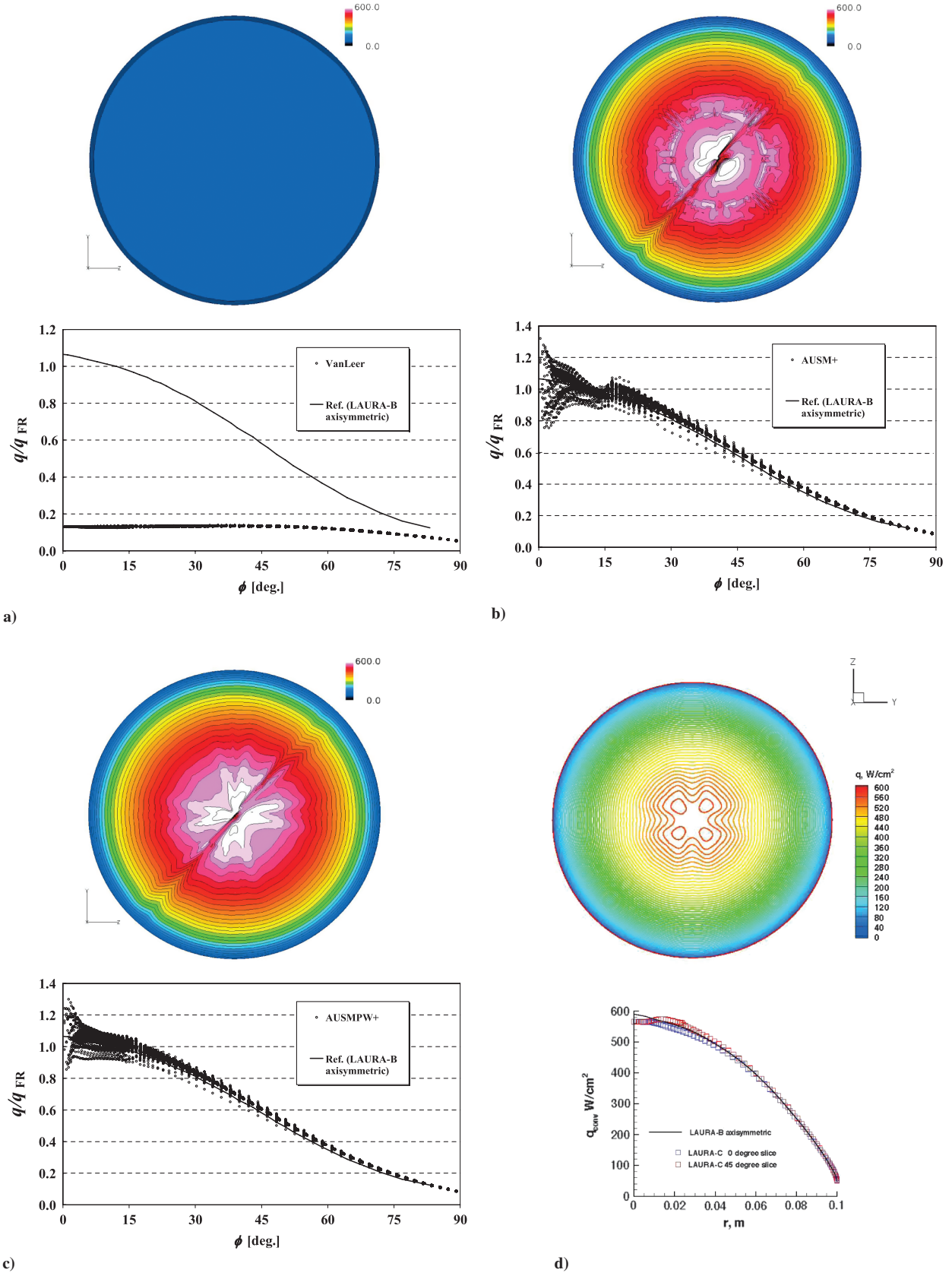

Fig. 25 Surface heating contours (top; $0 < q < 600$ W/cm^2) and profiles (bottom; 3-D, sphere): a) Van Leer, b) AUSM+, c) AUSMPW+, and d) [15], courtesy of Gnoffo.

integration methods and entire code structures. In this sense, Gnoffo's latest updates [38] to his multidimensional flux would be promising thanks to multidimensional entropy fix, although it still seems to have left some exploration as a future challenge, especially in obtaining fully symmetric and accurate heating in the hypersonic sphere problem.

Figure 26 shows density residual histories of the present computations, and AUSM+ and AUSMPW+ exhibited around three

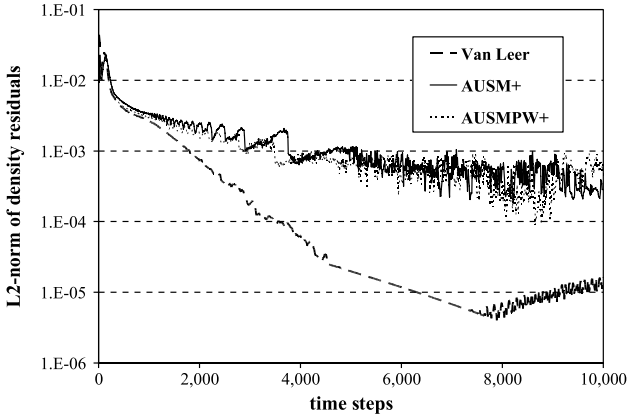

Fig. 26 Residual histories for sphere ($M_\infty = 12$).

orders drop in the residual. From the engineering point of view, these solutions can be regarded as 'converged,' and thus we stopped our calculations (although even with this level of residual decrease, it is speculated that shock anomalies grow later [9]).

V. Conclusions

We made a comparative study on the behaviors of flux functions with regard to two- and three-dimensional shock anomalies (instabilities and oscillations). The following features are noteworthy for hypersonic flow computations in three dimensions.

A simple expectation that three-dimensional (3-D) shock anomalies always appear more likely than two-dimensional (2-D) counterpart turned out to be false. Rather, the development of shock anomalies is seen in every direction and quite complicated in three dimensions. For instance, in a 2-D setup in three dimensions (circular cylinder in 2-D), computations demonstrated the following:

1) A 3-D case that exhibited a 2-D carbuncle: The 'carbuncle' developed in the two-dimensional slice, while the shock 'oscillation' appeared in the third direction. These anomalies developed from the very beginning of the computation with the same growth rate.

2) 3-D cases that were stable in 2-D: Depending on the grids or flux functions, either the following two solutions were obtained: the totally symmetric solution or the stable, symmetric solution remained in the 2-D slice, whereas the shock 'oscillation' developed in the third direction.

Multidimensional dissipations considered in AUSMPW+ flux function worked to suppress anomalous behaviors in limited cases but were not effective for genuinely 2-D or a genuinely 3-D development of shock anomalies.

AUSM-type fluxes generally yielded satisfactory predictions of heating for a 2-D problem in three dimensions for a cylinder but not for a genuinely 3-D problem for a sphere.

It is demonstrated that multidimensional dissipation is effective but not perfectly. This is partly because such dissipation terms had been developed under 2-D considerations and partly because those terms do not always work successfully even in two dimensions. Consequently, a flux function showing good or fair robustness against the shock in two dimensions can either succeed or fail to reproduce acceptable solutions in three dimensions. Thus, when one attempts to test a flux function, it is recommended to keep in mind that investigations only in two dimensions are not enough to accurately predict behaviors of the flux in three dimensions. Therefore, although most of the existing Euler fluxes were designed based on one or two dimensions but readily extendable to three dimensions, their performances in 3-D are too complicated to be predicted from the 2-D counterparts. Any flux function that eventually emerges as universal will have to meet (at the very least) all of the tests presented here. These are enough to show that a great variety of effects are possible and that these are sensitive to many aspects of the computation. At the present stage, acceptable heating prediction may be made by carefully considering those aspects, with a great effort or only by an expert user.

Acknowledgments

This work is partly supported by the Japan Society for the Promotion of Science (JSPS). We are grateful to all their cooperation. We are grateful to Peter Gnoffo of NASA Langley Research Center for giving us computational grids used in the three-dimensional cases and for permission to present his numerical results as reference. We also thank Jeffery White and Bil Kleb, also of NASA Langley Research Center, for providing us with grids. The computational code was originally developed at Nagoya University, Japan, while the first author was under supervision of Yoshiaki Nakamura. Hiroaki Nishikawa of the National Institute of Aerospace gave us valuable comments. We thank their cooperation.

References

[1] Peery, K. M., and Imlay, S. T., "Blunt-Body Flow Simulations," *24th AIAA/SAE/ASME/ASEE Joint Propulsion Conference*, Boston, AIAA Paper 1988-2904, July 1988.

[2] Robinet, J.-Ch., Gressier, J., Casalis, G., and Moschetta, J.-M., "Shock Wave Instability and the Carbuncle Phenomenon: Same Intrinsic Origin?," *Journal of Fluid Mechanics*, Vol. 417, Aug. 2000, pp. 237–263.
doi:10.1017/S0022112000001129

[3] Coulombel, J. F., Benzoni-Gavage, S., and Serre, D, "Note on a Paper by Robinet, Gressier, Casalis & Moschetta," *Journal of Fluid Mechanics*, Vol. 469, Oct. 2002, pp. 401–405.
doi:10.1017/S0022112002001891

[4] Roe, P., "Vorticity Capturing," *15th Computational Fluid Dynamics Conference*, Anaheim, CA, AIAA Paper 2001-2523, June 2001.

[5] Ramalho, M. V. C., and Azevedo, J. L. F., "A Possible Mechanism for the Appearance of the Carbuncle Phenomenon in Aerodynamic Simulations," *48th AIAA Aerospace Sciences Meeting*, Orlando, FL, AIAA Paper 2010-872, Jan. 2010.

[6] Elling, V., "The Carbuncle Phenomenon is Incurable," *Acta Mathematica Scientia*, Vol. 29B, No. 6, 2009, pp. 1647–1656.
doi:10.1016/S0252-9602(10)60007-0

[7] Pandolfi, M., and D'Ambrosio, D., "Numerical Instabilities in Upwind Methods: Analysis and Cures for the 'Carbuncle' Phenomenon," *Journal of Computational Physics*, Vol. 166, No. 2, 2001, pp. 271–301.
doi:10.1006/jcph.2000.6652

[8] Barth, T. J., "Some Notes on Shock-Resolving Flux Functions Part 1: Stationary Characteristics," NASA TM 101087, 1989.

[9] Kitamura, K., Roe, P., and Ismail, F., "Evaluation of Euler Fluxes for Hypersonic Flow Computations," *AIAA Journal*, Vol. 47, 2009, pp. 44–53.
doi:10.2514/1.33735

[10] Kim, K. H., Kim, C., and Rho, O. H., "Cures for the Shock Instability: Development of a Shock-Stable Roe Scheme," *Journal of Computational Physics*, Vol. 185, No. 2, 2003, pp. 342–374.
doi:10.1016/S0021-9991(02)00037-2

[11] Kim, S. S., Kim, C., Rho, O. H., and Hong, S. K., "Methods for the Accurate Computations of Hypersonic Flows 1. AUSMPW+ Scheme," *Journal of Computational Physics*, Vol. 174, No. 1, 2001, pp. 38–80.
doi:10.1006/jcph.2001.6873

[12] Nishikawa, H., and Kitamura, K., "Very Simple, Carbuncle-Free, Boundary-Layer Resolving, Rotated-Hybrid Riemann Solvers," *Journal of Computational Physics*, Vol. 227, No. 4, 2008, pp. 2560–2581.
doi:10.1016/j.jcp.2007.11.003

[13] Shima, E., and Kitamura, K., "Parameter-Free Simple Low-Dissipation AUSM-Family Scheme for All Speeds," *AIAA Journal*, Vol. 49, No. 8, 2011, pp. 1693–1709.
doi:10.2514/1.J050905

[14] Roe, P. L., and Kitamura, K., "Artificial Surface Tension to Stabilize Captured Shockwaves," *38th Fluid Dynamics Conference*, Seattle, WA, AIAA Paper 2008-3991, June 2008.

[15] Gnoffo, P. A., "Multi-Dimensional, Inviscid Flux Reconstruction for Simulation of Hypersonic Heating on Tetrahedral Grids," *47th AIAA Aerospace Sciences Meeting*, Orlando, FL, AIAA Paper 2009-599, Jan. 2009.

[16] Loh, C. Y., and Jorgenson, P. C. E., "Multi-Dimensional Dissipation for Cure of Pathological Behaviors of Upwind Scheme," *Journal of Computational Physics*, Vol. 228, No. 5, 2009, pp. 1343–1346.
doi:10.1016/j.jcp.2008.10.044

[17] Phongthanapanich, S., and Dechaumphai, P., "Healing of Shock Instability for Roe's Flux-Difference Splitting Scheme on Triangular Meshes," *International Journal for Numerical Methods in Fluids*,

Vol. 59, No. 5, 2009, pp. 559–575.
doi:10.1002/fld.1834
[18] Huang, K., Wu, H., Yu, H., and Yan, D., "Cures for Numerical Shock Instability in HLLC Solver," *International Journal for Numerical Methods in Fluids*, Vol. 65, No. 9, 2011, pp. 1026–1038.
doi:10.1002/fld.2217
[19] Gnoffo, P. A., and White, J. A., "Computational Aerothermodynamic Simulation Issues on Unstructured Grids," *37th AIAA Thermophysics Conference*, Portland, OR, AIAA Paper 2004-2371, July 2004.
[20] Candler, G. V., Mavriplis, D. J., and Treviño, L., "Current Status and Future Prospects for the Numerical Simulation of Hypersonic Flows," *47th AIAA Aerospace Sciences Meeting*, Orlando, FL, AIAA Paper 2009-153, Jan. 2009.
[21] Kitamura, K., Shima, E., Nakamura, Y., and Roe, P., "Evaluation of Euler Fluxes for Hypersonic Heating Computations," *AIAA Journal*, Vol. 48, 2010, pp. 763–776.
doi:10.2514/1.41605
[22] Yoon, S. H., Kim, C., and Kim, K. H., "Multi-Dimensional Limiting Process for Three-Dimensional Flow Physics Analyses," *Journal of Computational Physics*, Vol. 227, No. 12, 2008, pp. 6001–6043.
doi:10.1016/j.jcp.2008.02.012
[23] Balsara, D. S., "Multidimensional HLLE Riemann Solver: Application to Euler and Magnetohydrodynamic Flows," *Journal of Computational Physics*, Vol. 229, No. 6, 2010, pp. 1970–1993.
doi:10.1016/j.jcp.2009.11.018
[24] "Hypersonic Benchmarks," FUN3D Manual, Chap. 9, http://fun3d.larc.nasa.gov/chapter-9.html#hypersonic_benchmarks [retrieved 4 June 2009].
[25] Van Albada, G. D., Van Leer, B., and Roberts, W. W., Jr., "A Comparative Study of Computational Methods in Cosmic Gas Dynamics," *Astronomy and Astrophysics*, Vol. 108, 1982, pp. 76–84.
[26] Van Leer, B., "Towards the Ultimate Conservative Difference Scheme. V. A Second-Order Sequel to Godunov's Method," *Journal of Computational Physics*, Vol. 32, No. 1, 1979, pp. 101–136.
doi:10.1016/0021-9991(79)90145-1
[27] Roe, P. L., "Approximate Riemann Solvers, Parameter Vectors, and Difference Schemes," *Journal of Computational Physics*, Vol. 43, No. 2, 1981, pp. 357–372.
doi:10.1016/0021-9991(81)90128-5
[28] Harten, A., "High Resolution Schemes for Hyperbolic Conservation Laws," *Journal of Computational Physics*, Vol. 49, No. 3, 1983, pp. 357–393.
doi:10.1016/0021-9991(83)90136-5
[29] Van Leer, B., "Flux Vector Splitting for the Euler Equations," *Lecture Notes in Physics*, Vol. 170, 1982, pp. 507–512.
doi:10.1007/3-540-11948-5_66
[30] Liou, M.-S., "A Sequel to AUSM: AUSM+," *Journal of Computational Physics*, Vol. 129, No. 2, 1996, pp. 364–382.
doi:10.1006/jcph.1996.0256
[31] Hänel, D, Schwane, R., and Seider, G., "On the Accuracy of Upwind Schemes for the Solution of the Navier–Stokes Equations," AIAA Paper 1987-1105, 1987.
[32] Men'shov, I. S., and Nakamura, Y., "Numerical Simulations and Experimental Comparisons for High-Speed Nonequilibrium Air Flows," *Fluid Dynamics Research*, Vol. 27, No. 5, 2000, pp. 305–334.
doi:10.1016/S0169-5983(00)00010-1
[33] White, J., et al., private communication, April 2007.
[34] Gnoffo, P., private communication, March 2009.
[35] Fay, J. A., and Riddell, F. R., "Theory of Stagnation Point Heat Transfer in Dissociated Air," *Journal of the Aerospace Sciences*, Vol. 25, No. 2, 1958, pp. 73–85.
doi:10.2514/8.7517
[36] Candler, G., Barnhardt, M., Drayna, T., Nompelis, I., Peterson, D., and Subbareddy, P., "Unstructured Grid Approaches for Accurate Aeroheating Simulations," *18th AIAA Computational Fluid Dynamics Conference*, Miami, FL, AIAA Paper 2007-3959, June 2007.
[37] Gnoffo, P., and Kleb, B., private communication, March 2009.
[38] Gnoffo, P. A., "Updates to Multi-Dimensional Flux Reconstruction for Hypersonic Simulations on Tetrahedral Grids," *48th AIAA Aerospace Sciences Meeting*, Orlando, FL, AIAA Paper 2010-1271, Jan. 2010.

W. Anderson
Associate Editor